THEORETICAL & APPLIED MECHANICS LETTERS **4**, 032004 (2014)

Three-dimensional numerical simulation of a vortex ring impacting a bump

Heng Ren,[1, a)] Changyue Xu[2, b)]
[1)]*China Electronics Technology Group Corporation No.38 Research Institute, Hefei 230031, China*
[2)]*College of Aerospace Engineering, Nanjing University of Aeronautics and Astronautics, Nanjing 210016, China*

(Received 15 January 2014; accepted 15 March 2014)

Abstract A vortex ring impinging on a three-dimensional bump is studied using large eddy simulation for a Reynolds number $Re = 4 \times 10^4$ based on the initial translation speed and diameter of the vortex ring. The effects of bump height on the vortical flow phenomena and the underlying physical mechanisms are investigated. Based on the analysis of the evolution of vortical structures, two typical kinds of vortical structures, i.e., the wrapping vortices and the hair-pin vortices, are identified and play an important role in the flow state evolution. The circulation of the primary vortex ring reasonably elucidates some typical phases of flow evolution. Furthermore, the mechanism of flow transition from laminar to turbulent state has been revealed based on analysis of turbulent kinetic energy.
 [doi:10.1063/2.1403204]

Keywords large eddy simulation, vortex ring, bump, vortical structure, turbulent state

As one of the typical forms of vortex motion, vortex rings widely exist in nature and engineering. The interaction of vortex rings with solid or fluid boundaries is a fundamental problem in fluid dynamics and has received considerable attention. This subject is also associated with a variety of practical applications, such as cavitated rings used for underwater drilling[1] and the downburst and aircraft interaction.[2] Moreover, the underlying flow phenomena and physical mechanisms are still unclear and are worthy of detailed studies.

Vortex ring interacting with a flat wall has been extensively studied.[3–8] These studies showed that as the primary vortex ring moves gradually toward the wall, its rate of approach slows down and its radius continues to increase. When the Reynolds number is larger than 500 based on the initial diameter and translational speed of the vortex ring, the formation of the secondary vortex ring occurs and then it impacts the primary one. Experimental study[3] has revealed that, beyond $Re = 3\,000$, the primary vortex ring will no longer remain stable as it approaches the wall. Thus, the instability and transition to turbulence for the vortex ring evolution should be considered when the Reynolds number becomes large enough.

For the instability of vortex rings, extensive investigations have been carried out. Krutzsch[9] first studied this subject and found that the vortex ring becomes unstable with some stationary waves distributed around its azimuthal direction. Then Maxworthy[10] verified experimentally that

[a)]Corresponding author. Email: renheng@mail.ustc.edu.cn.
[b)]Email: cyxu@nuaa.edu.cn.

the stationary azimuthal waves grow at 45° relative to the propagation direction of vortex ring, and the wave number depends on the slenderness ratio of core radius to ring radius. Widnall and Tsai[11] presented the theoretical explanation of the instability and indicated that a straining field in the neighbourhood of the vortex core leads to the amplification of small perturbation. Then Shariff et al.[12] established a viscous correction to the growth rate proposed by Widnall and Tsai[11] based on their direct numerical simulation (DNS) results.

Comparing with the numerous studies of vortex ring interacting with a flat surface, the investigation relevant to a vortex ring impacting a curved wall is scarce. Orlandi and Verzicco[13] numerically studied vortex pairs interacting with a two-dimensional circular cylinder with no-slip and free-slip boundary conditions. For the free-slip condition, the dipole is observed to split into two vortices and then to rejoin on the cylinder. While for the no-slip interaction, the generation of dipolar and tripolar structures occurs on the cylinder surface. Verzicco et al.[14] further studied this problem. They found that the induced vortices become more apparent as the diameter of the cylinder increases. Recently, Sousa[15] studied a vortex ring impacting a stationary sphere for $Re = 1\,000$ using DNS. After the secondary vortex ring is formed, they found its interaction with the primary ring results in the fast decay of circulation for the secondary ring.

In this paper, a large eddy simulation (LES) technique is utilized to investigate the effects of bump height on the dynamics of vortical structures and the turbulent behaviors when a vortex ring impacts a three-dimensional bump at Reynolds number $Re = 4 \times 10^4$. To our knowledge, the relevant work has never been performed before. The purpose is to investigate the complex flow phenomena and the underlying mechanisms.

The compressible Navier–Stokes equations in generalized coordinates are solved using the LES coupled with dynamic subgrid-scale (SGS) models. As employed in our previous work,[16,17] the viscous terms and convective terms are discretized by a fourth-order and a second-order centered scheme, respectively. Moreover, the present numerical methods have already been employed successfully to a variety of turbulent flows[18–20] and have been verified the reliable calculations.

According to the schematic as depicted in Fig. 1, a Gaussian vortex ring[13] with radius R_0 is initially placed at $\boldsymbol{x}_c = (0, 0, H_v)$, where H_v is the distance between the vortex ring center and the bottom surface. The bump has a circular base with a cosine-squared cross section which is defined as $z(x, y) = H_b \cos^2(\pi\sqrt{x^2 + y^2}/6)$, where H_b is the bump height. The initial translational speed of the vortex ring can be represented as[21] $u_v = [\Gamma/(4\pi R_0)](\ln(8R_0/\sigma_0) - 1/4)$, where σ_0 is the initial core radius and Γ represents the circulation of the vortex ring. To deal with the instability of the vortex ring, an azimuthal disturbance with an amplitude of 2×10^{-4} is introduced by imposing a radial displacement on the axis of the ring.[12]

In the computation, the effect of bump height is investigated. The parameters of three cases are given as follows. For all the cases, the slenderness ratio and initial height of the vortex ring are $\sigma_0/R_0 = 0.2$[7,17] and $H_v/R_0 = 6R_0$, respectively, and the Reynolds number is $Re = 4 \times 10^4$. The bump height H_b/R_0 are 1.8, 2.4, and 3.0 for case 1, case 2, and case 3, respectively. The computational domain extends for $16R_0$ in the x and y directions and $12R_0$ in the z or vertical direction, i.e., $L_x/R_0 = L_y/R_0 = 16$, $L_z/R_0 = 12$. Based on our careful examinations, a mesh of size $N_x \times N_y \times N_z = 641 \times 641 \times 321$ with a resolution $R_0 = 40\Delta x$ is used in the computation. The grid-spacing is uniform in the x–y plane, and a grid stretching in the vertical direction is used to

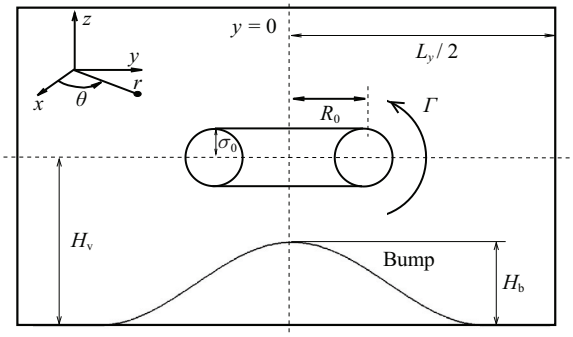

Fig. 1. Schematic diagram of a vortex ring approaching a bump.

increase the grid resolution near the surface. Periodic boundary conditions are used in the x and y directions. No-slip boundary condition is employed on the bump surface and a far-field boundary condition is applied in the $z = L_z$ plane.

We first investigate the evolution of vortical structures depicted in Fig. 2. For comparability of the vortical structures for cases 1–3 as shown in Fig. 2, it is indicated that the distances between the vortex ring center and the bump top are $0.32R_0$ approximately for case 1 at $T = 15.0$, case 2 at $T = 12.5$, and case 3 at $T = 10.0$. From Fig. 2(a) for case 1, when the primary vortex ring moves close to the bump, a vorticity layer is obviously generated on the core surface of bump at $T = 15.0$. Then the separation of boundary layer occurs and the secondary vortex ring is generated at $T = 17.5$. Due to the growth of the azimuthal perturbation, the primary ring develops into a wavy-like structure at $T = 17.5$ and 20.0. Furthermore, by means of Fourier analysis of the azimuthal perturbation, it is identified that the dominant mode of the instability for the primary ring is $k = 11$, consistent with the theoretical estimate of the dominant mode $k = 2.26/\sigma_0$ approximately by Maxworthy[10] and the number of the wavy-like structures observed at $T = 17.5$ and 20.0. After the primary ring collides with the bump surface, the secondary ring generated lifts up from the surface and then moves over the primary vortex ring. At $T = 22.5$, it is seen that the secondary ring has already moved up the primary ring. Subsequently, a variety of loop-like vortices wrapping around both the primary and secondary vortex rings (briefly called "wrapping vortices") are formed at $T = 25.0$ and 27.5. The generation of these wrapping vortices is associated with the azimuthal instability of the vortex rings.[22] Finally, the complicated interactions of the wrapping vortices and vortex rings over the bump surface result in the breakdown of the vortical structures into small-scale vortices at $T = 30.0$, and further lead to the vortical flow transition to turbulent state which will be analyzed below.

To investigate the effect of the bump height on the flow structures, Figs. 2(b) and 2(c) show the vortical structures for cases 2 and 3, respectively. The evolution of vortical structures for the generation of secondary vortex ring is similar to case 1. When the wavy-like secondary ring locates over the primary vortex ring, the secondary ring stretches significantly and causes severe distortion of the secondary ring at $T = 20.0$ for case 2 in Fig. 2(b) and $T = 17.5$ for case 3 in Fig. 2(c). Then, the intense stretching effect results in the disconnection of the secondary ring and the generation of "hair-pin vortices" at $T = 22.5$ for case 2 and $T = 20.0$ for case 3. These hair-pin

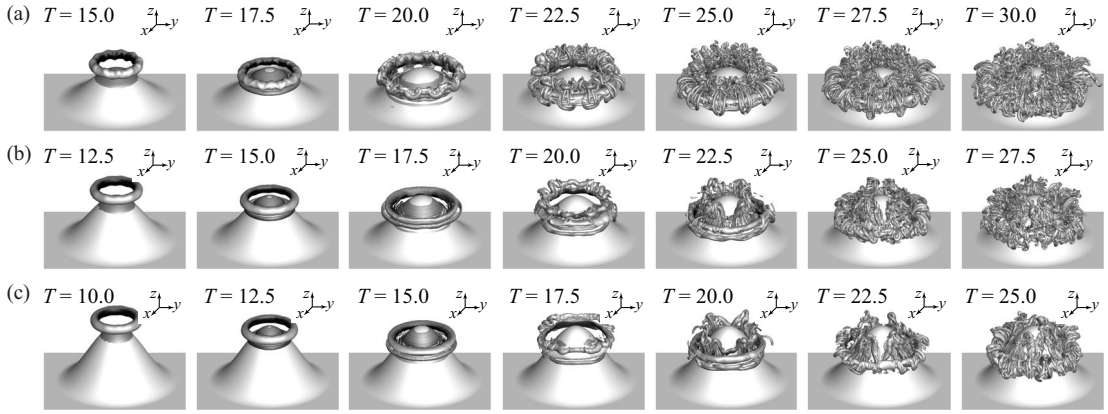

Fig. 2. Evolution of vortical structures depicted by iso-surface of the Q criterion with $Q = 0.5$: (a) case 1, (b) case 2, (c) case 3.

vortices evolve over the bump surface because of the induction of the primary vortex ring. When the hair-pin vortices collide with the surface, the vortices break into small-scale ones and move upwards over the bump surface at $T = 25.0$ for case 2 and $T = 22.5$ for case 3. Subsequently, the interactions of the hair-pin vortices and vortex rings over the bump surface result in the flow transition.

Further, to quantitatively analyze the development of azimuthal instabilities for the vortex rings, we perform the Fourier decomposition of the vertical vorticity ω_z and get $\bar{A}_k$,[15] which denotes the azimuthal perturbation in the vortical structures. The evolution of $\bar{A}_k$ for the primary vortex ring in case 1 is plotted in Fig. 3. At $T = 15.0$, the vorticity component in the wall-normal direction ω_z appears and it is obvious that the dominant mode is $k = 11$, consistent with the vortical structures shown in Fig. 2(a). With the evolution of the vortex ring, the amplitude of ω_z increases rapidly implying the fast growth of the instability. At $T = 20.0$, the second harmonic $k = 22$ is apparent and the amplitude of $\bar{A}_k$ increases considerably, as shown in Fig. 3(b). Then with the vertical vorticity ω_z breaking into small-scale vorticity, the dominant and second harmonic modes decay rapidly, as depicted in Figs. 3(c) and 3(d).

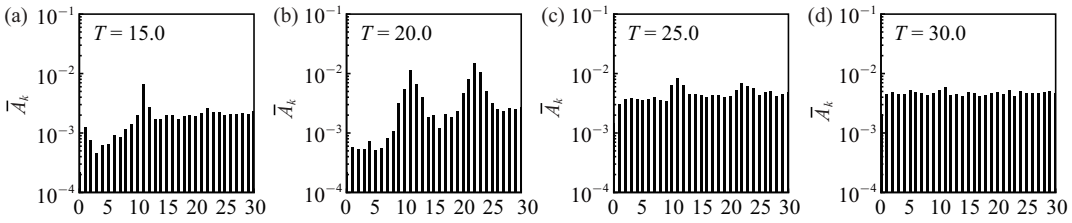

Fig. 3. Azimuthal perturbation of primary vortex ring for case 1.

We then study the circulation of the primary ring and the total kinetic energy in the flow field. Here, the circulation is calculated by $\Gamma = \int \langle \omega_\theta \rangle \, dr \, dz$,[22] where the integration domain for the primary vortex ring is chosen as the region with $\langle \omega_\theta \rangle < 0$,[12] the symbol "$\langle\rangle$" represents the average in the azimuthal direction after transforming the data from the Cartesian coordinate to

the cylindrical coordinate system. Furthermore, the total kinetic energy can be written as $E = (1/2)\int(\bar{\boldsymbol{u}}\cdot\bar{\boldsymbol{u}})\,\mathrm{d}V$, where the integral domain is the whole flow field and $\bar{\boldsymbol{u}}$ represents the resolved velocity.

The circulation is shown in Fig. 4(a). Based on the profiles for all the cases, the evolution of circulation can be divided into three phases. Firstly, as the vortex ring is away from the bump, the circulation is nearly constant. Then the interaction of the vortex ring with the bump occurs and the circulation decreases quickly. Thirdly, after the vortices break up into small-scale ones, the strength of vortex ring becomes relatively weak and the circulation decreases slowly. As the bump height increases, the decay rate of circulation decreases. This behavior is attributed to a weaker interaction between the primary vortex ring and the surface when H_b increases.

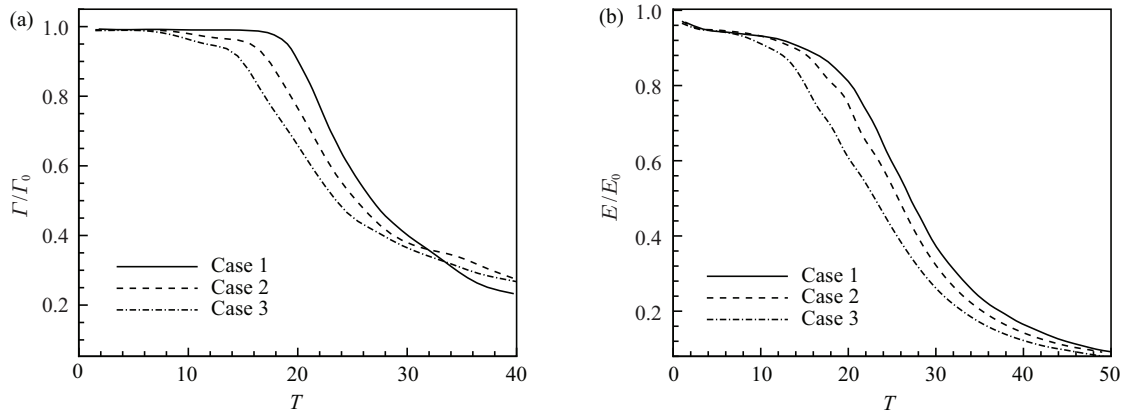

Fig. 4. (a) Circulation of the primary ring and (b) total kinetic energy in the flow field.

Figure 4(b) depicts the evolution of total kinetic energy, where E_0 represents the initial kinetic energy. It can be seen that the kinetic energy decreases slowly due to viscous dissipation before the vortex ring collides with the bump surface. Then the kinetic energy deceases quickly as the vortex-surface interaction. With the increase of the bump height, the decay rate of the kinetic energy becomes smaller, consistent with the evolution of circulation shown in Fig. 4(a).

Finally, we investigate the flow transition from laminar to turbulent state and the relevant turbulent behavior. The turbulent kinetic energy (TKE) is defined as $E_\mathrm{TKE} = (1/2)\int(\boldsymbol{u}'\cdot\boldsymbol{u}')\,\mathrm{d}V$, where $\boldsymbol{u}'$ represents the velocity fluctuations and is defined as $\boldsymbol{u}' = \bar{\boldsymbol{u}} - \langle\bar{\boldsymbol{u}}\rangle$, and the integral domain is the whole flow field.

Figure 5 shows the evolution of E_TKE. Before the vortex ring interacts with the bump, the turbulent kinetic energy vanishes, corresponding to laminar flow state. As a typical example, we mainly discuss the behavior for case 1. It is identified that the generation of secondary vortex ring at $T = 17.5$ approximately is an indication of the growth of E_TKE. Then with the development of the azimuthal instability in the vortical structures and the breakdown of these vortices, the E_TKE grows rapidly and reaches its maximum at approximately $T = 28$, representing the flow transition to turbulence.[23,24] After $T = 28$, the E_TKE decays quickly due to the vortical evolution and viscous decay. Moreover, compared with the three cases, as the bump height increases, the maximum of E_TKE decreases gradually in Fig. 5.

According to the investigation of an isolated vortex ring by Archer et al.,[22] the shedding of hair-pin vortices along the azimuthal direction of the ring indicates turbulent flow state. In this study, two typical vortical structures are identified. As both the wrapping and hair-pin vortices are mainly distributed by the vorticity components in the radial and vertical directions, we can reasonably measure the strength of these vortices by integrating the enstrophy in the whole flow field, $\Omega_{rz} = (1/2)\int(\omega_r^2 + \omega_z^2)\mathrm{d}V$, where ω_r and ω_z represent the vorticity components in the radial and vertical directions, respectively.

The evolution of Ω_{rz} is shown in Fig. 6. Compared with the profiles of E_{TKE} in Fig. 5, it is interesting to notice that the time-dependent characters of both Ω_{rz} and E_{TKE} exhibit the similar manner. The generation of Ω_{rz} (or the wrapping vortices and hair-pin vortices) corresponds to the instant of the growth of E_{TKE}. This behavior reasonably indicates that the formation of the wrapping and hair-pin vortices plays an important role in the flow transition.

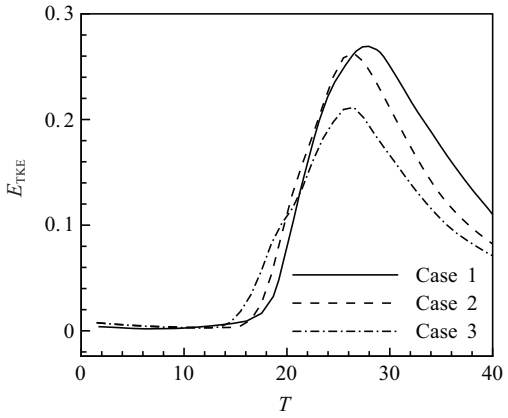

Fig. 5. Evolution of turbulent kinetic energy integrated over the whole domain.

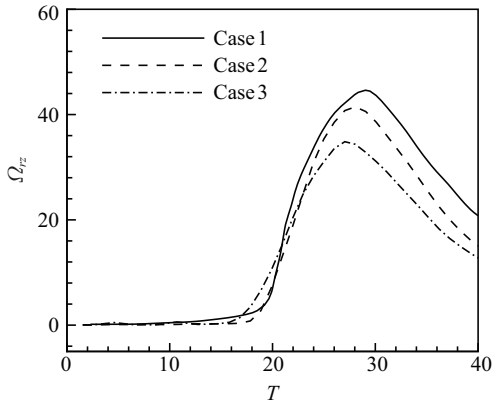

Fig. 6. Evolution of the enstrophy of wrapping and hair-pin vortices integrated over the whole domain.

In summary, the interaction between a vortex ring and a three-dimensional bump has been studied by means of an LES technique. The effects of bump height on the vortical flow phenomena and the underlying physical mechanisms were investigated. Two typical kinds of vortical structures are identified and briefly represented as the wrapping vortices and the hair-pin vortices. The circulation of the vortex ring and the total kinetic energy have been investigated to reveal the different stages of flow evolution. The evolution of circulation can be divided into three phases. Firstly, as the vortex ring is far away from the bump, the circulation is nearly constant. Then the interaction of the vortex ring with the bump occurs and the circulation decreases quickly. Thirdly, after the vortices break up into small-scale ones, the circulation decreases slowly. Moreover, the evolution of TKE and enstrophy has been analyzed. It is found that the formation of the wrapping and hair-pin vortices plays an important role in the flow transition from laminar to turbulent state.

This work was supported by the National Natural Science Foundation of China (11202100) and the Natural Science Fund in Jiangsu Province (BK2011723).

1. G. L. Chahine, P. F. Genoux. Collapse of a cavitating vortex ring. *Journal of Fluids Engineering* **105**, 400–405 (1983).
2. T. S. Lundgren, N. N. Mansour. Vortex ring bubbles. *Journal of Fluid Mechanics* **224**, 177–196 (1991).

3. J. D. A. Walker, C. R. Smith, A. W. Cerra, et al. The impact of a vortex ring on a wall. *Journal of Fluid Mechanics* **181**, 99–140 (1987).
4. C. C. Chu, C. T. Wang, C. C. Chang. A vortex ring impinging on a solid plane surface-vortex structure and surface force. *Physics of Fluids* **7**, 1391–1401 (1995).
5. P. Orlandi. Vortex dipole rebound from a wall. *Physics of Fluids A* **2**, 1429–1436 (1990).
6. H. J. H. Clercx, C. H. Bruneau. The normal and oblique collision of a dipole with a no-slip boundary. *Computers & Fluids* **35**, 245–279 (2006).
7. M. Cheng, J. Lou, L. S. Luo. Numerical study of a vortex ring impacting a flat wall. *Journal of Fluid Mechanics* **660**, 430–455 (2010).
8. L. D. Couch, P. S. Krueger. Experimental investigation of vortex rings impinging on inclined surfaces. *Experiments in Fluids* **51**, 1123–1138 (2011).
9. C. Krutzsch. Über eine experimentell beobachtete erscheining an werbelringen bei ehrer translatorischen beivegung in weklechin, flussigheiter. *Annln Physics* **5**, 497–523 (1939) (in Germany).
10. T. Maxworthy. The structure and stability of vortex rings. *Journal of Fluid Mechanics* **51**, 15–32 (1972).
11. S. E. Widnall, C. Y. Tsai. The instability of the thin vortex ring of constant vorticity. *Philosophical Transactions of the Royal Society of London A* **287**, 273–305 (1977).
12. K. Shariff, R. Verzicco, P. Orlandi. A numerical study of three-dimensional vortex ring instabilities: viscous corrections and early nonlinear stage. *Journal of Fluid Mechanics* **279**, 351–375 (1994).
13. P. Orlandi, R. Verzicco. Vortex rings impinging on walls: axisymmetric and three-dimensional simulations. *Journal of Fluid Mechanics* **256**, 615–646 (1993).
14. R. Verzicco, J. B. Flor, G. J. F. Van Heijst, et al. Numerical and experimental study of the interaction between a vortex dipole and a circular cylinder. *Experiments in Fluids* **18**, 153–163 (1995).
15. P. J. F. de Sousa. Three-dimensional instability on the interaction between a vortex and a stationary sphere. *Theoretical and Computational Fluid Dynamics* **26**, 391–399 (2012).
16. C. Y. Xu, L. W. Chen, X. Y. Lu. Large eddy simulation of the compressible flow past a wavy cylinder. *Journal of Fluid Mechanics* **665**, 238–273 (2010).
17. H. Ren, X. Y. Lu. Large eddy simulation of a vortex ring impinging on a three-dimensional circular cylinder. *Theoretical & Applied Mechanics Letters* **3**, 032007 (2013).
18. X. Y. Lu, S. W. Wang, H. G. Sung, et al. Large-eddy simulations of turbulent swirling flows injected into a dump chamber. *Journal of Fluid Mechanics* **527**, 171–195 (2005).
19. L. W. Chen, C. Y. Xu, X. Y. Lu. Numerical investigation of the compressible flow past an aerofoil. *Journal of Fluid Mechanics* **643**, 97–126 (2010).
20. L. W. Chen, G. L. Wang, X. Y. Lu. Numerical investigation of a jet from a blunt body opposing a supersonic flow. *Journal of Fluid Mechanics* **684**, 85–110 (2011).
21. P. G. Saffman. The number of waves on unstable vortex rings. *Journal of Fluid Mechanics* **84**, 625–639 (1978).
22. P. J. Archer, T. G. Thomas, G. N. Coleman. Direct numerical simulation of vortex ring evolution from the laminar to the early turbulent regime. *Journal of Fluid Mechanics* **598**, 201–226 (2008).
23. M. Sreedhar, S. Ragab. Large eddy simulation of longitudinal stationary vortices. *Physics of Fluids* **6**, 2501–2514 (1994).
24. S. Ragab, M. Sreedhar. Numerical simulation of vortices with axial velocity deficits. *Physics of Fluids* **7**, 549–558 (1995).